

Article

Mangrove Inspired Anti-Corrosion Coatings

Miaomiao Cui ^{1,2}, Peng-Yuan Wang ¹, Zuankai Wang ^{2,*}  and Bin Wang ^{1,*}

¹ Shenzhen Institutes of Advanced Technology, Chinese Academy of Sciences, Shenzhen 518055, China; miaomicui2-c@my.cityu.edu.hk (M.C.); py.wang@siat.ac.cn (P.-Y.W.)

² Department of Mechanical Engineering, City University of Hong Kong, Hong Kong, China

* Correspondence: zuanwang@cityu.edu.hk (Z.W.); bin.wang@siat.ac.cn (B.W.)

Received: 8 October 2019; Accepted: 28 October 2019; Published: 1 November 2019



Abstract: Marine corrosion accounts for one-third of the total corrosion cost and has been one of the greatest challenges for modern society. Organic coatings are known as the most widely used protective means. An effective control of the transport of corrosive substances is the key to the anti-corrosion performance. In nature, the mangrove survives and thrives in marine tidal zones despite high salinity and humidity. We first showed that the mangrove leaves have salt glands that can secrete excessive ions to control the ion transport in and out. Inspired by this, we proposed a design of bio-inspired, anti-corrosion coating that mimics this functional feature, and fabricated the bipolar, hydrophobic coatings by doping ion-selective resins and constructing surface structures, which restrict the transport of corrosive substances and the electrochemical corrosion at the coating/metal interface. Our results show that the bio-inspired coatings effectively block and control the transport of both the Na⁺ and Cl⁻, and, together with the hydrophobic surface, the coating system exhibits significantly improved anti-corrosion properties, more than a three orders of magnitude decrease in corrosion current density when compared with the control group (epoxy varnish). Therefore, the mangrove-inspired coatings show a promising protective strategy for the ever-demanding corrosion issues plaguing modern industries.

Keywords: bio-inspiration; anti-corrosion coating; salt gland; mangrove

1. Introduction

Corrosion, often metal corrosion, is the material destruction that leads to failure in function. It has been a major problem plaguing mankind dating back to ancient times. The first written description of corrosion appeared in the works of Plato (427–347 B.C.) [1] and the first patent of a protective paint appeared in 1625 [2]. Since a large number of metallic materials are developed and utilized in various fields such as marine oil and gas exploitation and transportation industries, the accompanying problem of corrosion becomes greater, which brings enormous economic loss and poses great threats to personal safety and the natural environment. According to the National Association of Corrosion Engineers International study 2016, the direct global corrosion cost was estimated to be \$2.5 trillion, which is equivalent to roughly 3.4% of the global Gross Domestic Product [3]. This study also reported that implementing corrosion control/prevention practices could result in savings of 15%–35% of the cost of damage. Among a variety of anti-corrosion techniques including the passive coatings and active methods [4], organic anti-corrosion coatings, which isolate and protect the substrate metal kinetically, are the most cost-effective and environmentally-friendly approach for the ever-pressing corrosion issue [5].

The fundamental principles of corrosion reveal that material corrosion is thermodynamically spontaneous and kinetically mediated by corrosive substances such as H₂O, Na⁺, and Cl⁻. These substances invade and transport through the coating to the coating/substrate interface, which leads

to an accelerated corrosion reaction [6] that consists of chemical corrosion and electrochemical corrosion. Moreover, the electrochemical corrosion processes at a high rate and it is a complex process that includes anodic and cathodic reactions. The anodic reaction transfers metal atoms into metal cations. This process can be accelerated by Cl^- , especially the pitting corrosion process [7,8]. On the other hand, the cathodic reaction generates OH^- followed by the aggregation of Na^+ , and this process could accelerate the accumulation of corrosion products, which leads to peeling-off of the coating [9,10]. These reactions, supplied by the penetrated corrosive substances, not only consume the metal substrate but also lead to the failure of the protective coatings. Therefore, the key to high-performance anti-corrosion coatings requires effective blocking of corrosive substances at the external surface and control of ion transportation within the coating [11–13].

Among the rapid research progress in protective coatings, learning from nature to design novel anti-corrosion materials is one of the best ways for creating these materials. Over the course of evolution, nature develops ingenious strategies that can be implemented to address the issues of surface blocking and ion control in anti-corrosion coatings. One representative dealing with the blocking is the superhydrophobic coating bio-inspired from self-cleaning lotus leaves, which protects metals from corrosion and has been studied extensively. The mechanism involves an isolative air layer formed between the external corrosive solution and the substrate, usually fulfilled by the hierarchical structure and the chemical constituents of the coating. Once the corrosive medium penetrates into the coating as time goes by, controlling the transportation of corrosive ions becomes significant to delay and, thus, prevent a corrosive reaction. Research efforts in controlling the transmission of corrosive agents can be passive, e.g., by adding fillers, such as zinc particles [14]. The mechanism involves the blocking and prolonging of the path of corrosive agents, and the preferred corrosion of zinc rather than steel due to a higher electrochemical activity. The other is an active approach that includes combining with conductive/reactive components to identify and interact with the ions selectively. A variety of ion-selective organic coatings doped with different ion exchange resins, first studied by Wang et al. [15–17], show effective control of the moving direction of ions such as Cl^- and Na^+ . The ion-selective coating that interacts with one type of ions is called single polar coating. An anionic coating (cation-selective film) blocks the invasion of anions (e.g., Cl^-) and allows the passage of cations (e.g., Na^+), while a cationic coating blocks the transmission of cations. A bipolar coating composed of cationic and anionic layers, which can restrict both types of ions, shows promising application in metal protection. Besides, conductive polymers, such as polyaniline (PANI) and modified PANI [18], have also been used for ion selective anti-corrosion coatings [8]. However, the ion selective coatings can only adjust the transport of ions and cannot deal with the water infiltration, which deteriorate the protective function of the coatings greatly. Therefore, preventing the invasion of H_2O into the coating layer is another important consideration of developing advanced anti-corrosion coatings.

Effective control of ion-containing fluids can also be observed in nature, e.g., the mangrove plants which survive and thrive in the marine intertidal environments featuring high humidity and high salinity through salt secretion [19]. The harsh habitat is close to the anti-corrosion coatings that protect the substrate metals in marine surroundings [20], and the strategies utilized by the mangrove through salt glands are vivid inspirations for developing ion-control coatings, formulated first in this work. In an aim to develop high-performance anti-corrosion coatings addressing the control of ion transport and external blocking, we explore the salt secretion of the mangrove, and, for the first time, fabricate mangrove-inspired anti-corrosion coatings employing ion-selective resins and hydrophobic surface construction. The structural and functional features of the salt glands on the mangrove (*Ceriops tagal* (perr.) C. B. Rob) are presented, and the bio-inspired, bipolar hydrophobic coatings were fabricated to exclude external H_2O and corrosive ions (Cl^- and Na^+). Our results show that the bio-inspired anti-corrosion coatings exhibit excellent properties in restraining the corrosive ion intrusion and transport within the coating, which leads to significantly improved anti-corrosion performance.

2. Materials and Methods

2.1. Observation of the Mangrove Leaves

The optical images of living mangrove were taken by a digital camera. Mature mangrove (*Ceriops tagal* (perr.) C. B. Rob) leaves and some branches of the mangrove were collected from Shenzhen Bay. The mangrove branches were cultured in nutrition solutions that were diluted by 100 mL tap water and 100 mL 3.5 wt % NaCl solution, respectively, for eight days.

For scanning electron microscopy, mangrove leaf samples were sputter-coated using a Leica EM ACE200 Automatic low vacuum coating apparatus (platinum, 30 s) (Leica, Wetzlar, Germany), and then observed by a ZEISS SUPRA55 Field emission sweep electron microscope (Carl Zeiss, Jena, Germany). The elemental mappings through energy-dispersive X-ray spectroscopy (EDS) of the samples were scanned by an Oxford X-Max 20 Electrically cooled X-ray spectrometer (Oxford, England).

2.2. Fabrication of the Mangrove-Inspired Coatings

Epoxy varnish (E-44 bisphenol A epoxy resin) was used as the film forming material. Single-polar coatings (two types) were obtained by doping different ion-selective resins, the 719 (202) strong base styrene anion exchange resin, and the 732 strong acid styrene cation exchange resin, respectively, into the epoxy varnish as paints. The ion exchange resins and epoxy varnish were diluted by xylene, and the doping concentrations were 0, 2.5 wt %, 5 wt %, 10 wt %, and 20 wt % for both groups. After the paints were evenly distributed in the epoxy varnish, TY-650 polyamide was mixed to cure the epoxy varnish. Then they were brush-coated on silica gel plate and also metal substrates (Q235) to obtain the single-polar coatings and the coated metal samples, respectively.

Q235 steel with the size of 10 mm × 10 mm × 5 mm was the metal substrate and the main elements are (wt %), C 0.127, Si 0.15, Mn 0.41, P 0.018, S 0.019, Fe balance. All metal substrates were polished with water on graded sandpapers (150#, 400#, 600#, 800#, and 1000#) step-by-step and were linked with copper wire by soldering. Metal samples were sealed by epoxy resin with a working surface of 10 mm × 10 mm exposed. Sealed samples were polished with water phase sandpapers (150#, 400#, 600#, 800#, and 1000#,) step-by-step, washed by anhydrous ethanol, dried, and kept in a dryer until utilization.

For the bipolar, hydrophobic coatings, a hydrophobic surface layer was fabricated using a template method. A superhydrophobic silicon plate was fabricated following the method in previous work [21,22]. The silicon nanowires and grooves were fabricated based on a 425-mm thick silicon wafer. A standard Micro-Electro-Mechanical System process technology was employed to fabricate rough structures on a silicon surface, which consists of two essential structural features, silicon micropillars, and silicon grooves. A photolithography process was first used to selectively cover a photoresist on a silicon wafer, which was followed by reactive ion etching (RIE) to etch the wafer areas that are not protected by the photoresist, and deep RIE was used to further etch the silicon substrate. This process formed silicon micropillars. The deep RIE process included cyclic passivation and etching modes in which C4F8 and SF6 were used. In the etching cycle, the SF6 flow rate was 130 sc-cm and platen power was set at 12 W. In the passivation cycle, the C4F8 flow rate was 85 sc-cm. Lastly, the photoresist was removed and deep RIE was used to further etch the silicon substrate covered by photoresist, which formed a silicon groove. Then, the surface fabrication process was completed. The prepared silicon wafer was taken as an original template, and PDMS was applied to copy the structure on the coating surface. The thicknesses of all fabricated coatings were measured by a micrometer. The thicknesses of bare metal substrates were monitored at three different points, and the average of all the measurements was taken as the thickness of metals (TM). The total thickness of coatings and metal substrate (TT) were measured by the same processes. Then the thickness of the coating is the difference of the TT and the TM. For the first type of single polar coatings, the coating thicknesses of the fabricated coatings and control groups were kept the same ($45 \pm 5 \mu\text{m}$). For the second type of bipolar coatings, the total coating thicknesses of the fabricated bipolar coatings and control groups were kept the same ($90 \pm 5 \mu\text{m}$), since those were fabricated layer-by-layer.

2.3. Electrochemical Measurements

Electrochemical tests including open circuit potential (OCP), electrochemical impedance spectroscopy (EIS), and polarization curves were performed on CHI760E. The electrochemical experiments were carried out in 3.5 wt % NaCl aqueous solution and a three-electrode configuration was applied, including the as-prepared samples (Q235 steel coated with the epoxy varnish, the bioinspired single-polar coatings, and the bioinspired bipolar, hydrophobic coatings), platinum plate, and saturated calomel electrode (SCE) as working, counter, and reference electrodes, respectively. If there is no other specific indication, all potentials reported in this paper are taking SCE as the reference. EIS tests were performed in a frequency range of 10^5 through 0.01 Hz at the open circuit potential with an amplitude of 10 mV. Potentiodynamic polarization curves were obtained by setting the sweeping range of ± 300 mV versus the rest potential value, and a rate of 1 mV/s was employed for scanning. The measured results were further analyzed by using software Cview.

2.4. Wettability and Ion-Resistant Property

The surface wettability was measured using a contact angle meter (DSA-100, KRÜSS Instruments, Hamburg, Germany) recording the contacting scenario of a water droplet to the surface. For the ion-selectivity analysis, the fabricated single-polar coatings were fixed in a custom-designed equipment, as shown in Figure 5a, between the 3.5 wt % NaCl solution (30 mL) on the left side and the ultrapure water (100 mL) on the right side. With increasing time at fixed intervals, 100 μ L solution on the left side was taken out and the concentrations of Cl^- and Na^+ were measured by ion chromatography (ICS-900, DIONEX, Sunnyvale, CA, USA) and inductively coupled the plasma mass spectrometer (iCAP Q, Thermo Scientific, Bremen, Germany).

3. Results and Discussion

3.1. Salt Particles Deposited on Mangrove Leaves and Salt Gland

Mangrove plants live along the marine coast sustaining the high salinity of seawater (living mangrove forest shown in Figure 1a). On the mangrove leaves, there are plenty of deposited particles (Figure 1b). To analyze the elements of the deposited particles, EDS was used and the results show that the main elements are Cl and Na with an atom ratio of approximately 1 (Figure 1c–e). Thus, the deposited particles are mainly NaCl particles. As reported in references [23–26], salt glands on the mangrove leaves can secrete salt solution to adapt to the harsh environment. However, the salt contained in the marine atmosphere can also be deposited on leaves. To further explore the source of the salt particles, we washed the fresh leaves (growing on branches) with distilled water to remove the deposited particles and cultured the collected branches in nutrition solutions diluted by tap water (NTW) and 3.5 wt % NaCl (NSW), respectively. After eight days, the cultured leaves were collected. The optical images of mangrove leaves cultured in NTW and NSW are shown in Figure 2a,b respectively. There are plenty of particles on leaves cultured in NSW, while no clear deposited particles on leaves cultured in NTW were observed. The same results can be seen in SEM images, as shown in Figure 2c,d with more particles observed in the sites of salt glands. EDS was applied and the results (Figure 2e,f) show that the deposited particles are NaCl. Thus, we conclude that, even though there may be two sources for the deposited salt particles on the fresh mangrove leaves, the salt glands of the mangrove leaves within the salted environment perform salt secretion well, which results in salt particles deposited on the leaf surfaces.

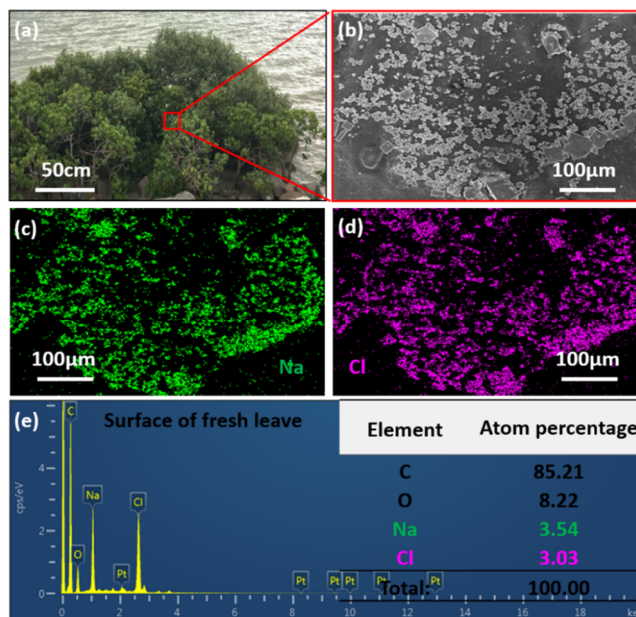


Figure 1. The mangrove and the deposited salt on the surface of fresh mangrove leaves. (a) The natural mangrove plants along the Shenzhen Bay. (b) SEM of the deposited salt on mangrove leaves, (c), (d) and (e) EDS of the deposited salt particles.

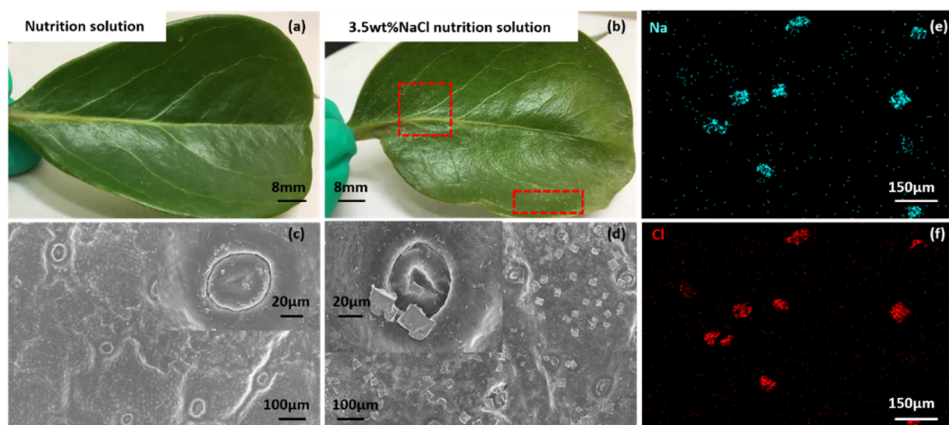


Figure 2. The deposited salt on the surface of cultured mangrove leaves. (a) and (b) are mangrove leaves cultured by nutrition solution and 3.5 wt. % NaCl nutrition solution, respectively. (c) and (d) are SEM images of mangrove leaves deposited with salt particles and the inserted images are the salt glands of mangrove leaves. (e) and (f) are EDS of the deposited salt particles.

Salt glands on mangrove leaves are multi-cellular tissues typically including cell types differentiated into basal collecting cells and distal secretory cells. The collecting cells are presumed to create a salt efflux gradient to collect salt from neighboring mesophyll cells and transport it to the secretory cells. The secretory cells are completely surrounded by a cuticle, with the exception of where they contact the subtending basal collecting cells, which is a feature that appears to channel the flow of salt through the secretory cells and prevent leakage back into the neighboring tissue via the apoplast [27]. We observe salt glands on both the top and lower surfaces of the mangrove leaves, as shown in Figure 3a,b. The magnified image (Figure 3d) of the salt gland shows that it is different from the stoma (breathing tissue). Based on the results we observed, we made a schematic illustration of salt gland distribution on the mangrove leaves. Salt glands function as a safety guard to control the ion transport into and out of the leaf to maintain healthy. From the perspective of bio-inspiration, this function is also necessary for an effective anti-corrosion coating, as well as needed to control the transport of corrosive ions and

water within the coating system. For this aim, we design and fabricate mangrove-inspired protective coatings that inhibit and control the transport of corrosive ions.

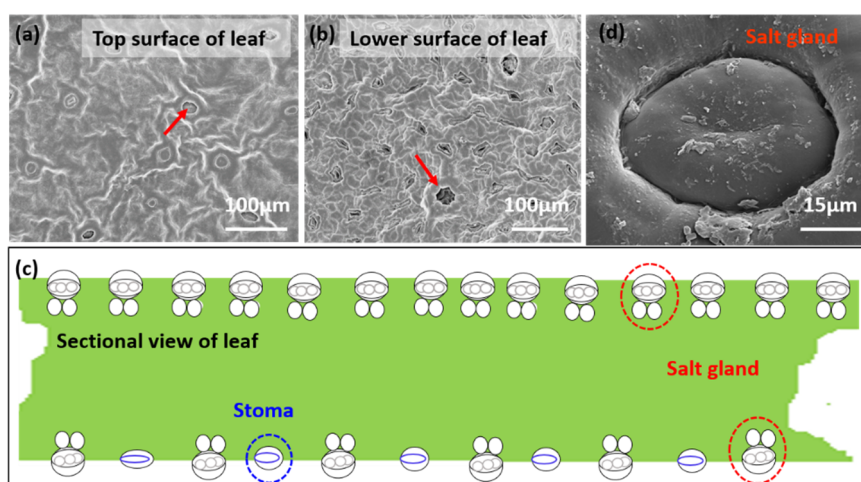


Figure 3. Salt glands distributed on the top and lower surfaces of mangrove leaves. (a) and (b) are morphologies of mangrove leaves on both surfaces. (c) Schematic illustration of the distribution of the salt glands on mangrove leaves. (d) SEM image of the salt gland on mangrove leaves.

3.2. Design and Properties of Mangrove-Inspired, Single-Polar and Bipolar Coatings

As ions diffuse/transport from a high concentration to a low concentration without external energy input/interference, we employed doping pigment materials that react with ions to resist or reduce this tendency. Ion exchangeable pigments have been applied in organic coatings to improve the anti-corrosion performance by preventing the transport of corrosive ions. In this case, we chose two types of commercial ion-exchange resins (719 (202) strong-base styrene anion exchange resin and 732 strong acid styrene cation exchange resin) as pigments to modify the epoxy varnish, which can function as inhibiting corrosive ions.

Anion exchange resin has positive charges that exclude cationic ions. Thus, doping anion exchange resin into epoxy can obtain a coating that blocks cations and we call this coating as cationic coatings, as illustrated in Figure 4a. Similarly, doping cation exchange resin can obtain anionic coatings (Figure 4b). These bio-inspired, single-polar coatings, with different doping concentrations, were tested by performing potentiodynamic polarization curves to find the optimized percentage, as shown in Figure 4c,d and Tables 1 and 2. It is clear that Q235 covered with epoxy varnish has decreased corrosion current density compared with the bare substrate, while the anti-corrosion property was further improved by the single-polar, cationic coatings. The lowest current density of Q235 protected with the cationic coating was $1.0091 \times 10^{-7} \text{ A/cm}^2$, which corresponds to a doping concentration of 10 wt % of anion exchange resin. Similarly, the single-polar, anionic coatings also showed enhanced anti-corrosion properties compared with the epoxy varnish on the Q235 substrate, and the optimal doping amount was 5 wt % of cation exchange resin.

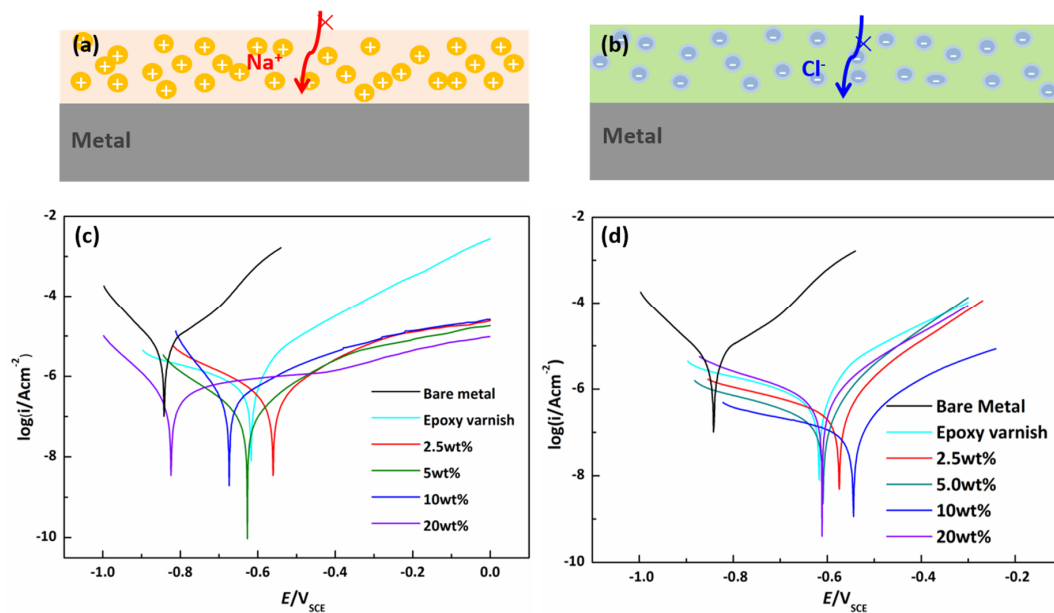


Figure 4. The single-polar, ion-selective coatings and the protective performance. (a) and (b) are the schematic illustrations of the repulsion function of the cationic coating and anionic coatings. (c) and (d) are potentiodynamic polarization curves of the cationic and anionic coatings with different doping concentrations of anion and cation exchange resins.

Table 1. Fitting results of Q235 steel coated with cationic coatings with different concentrations of anion exchange resin.

Parameters	Bare Metal	Epoxy Varnish	2.50 wt %	5.00 wt %	10.00 wt %	20.00 wt %
E_{corr}/V	-0.84156	-0.6171	-0.56056	-0.6270	-0.674	-0.82369
I_{corr}/Acm^{-2}	3.1212×10^{-6}	6.1134×10^{-7}	4.2421×10^{-7}	1.2796×10^{-7}	3.0586×10^{-7}	4.6885×10^{-7}
$R_p/\Omega cm^2$	2.6962×10^5	8.9052×10^5	1.3214×10^6	4.9000×10^6	2.2036×10^6	1.7568×10^6

Table 2. Fitting results of Q235 steel coated with anionic coatings with different concentrations of cation exchange resin.

Parameters	Bare Metal	Epoxy Varnish	2.50 wt %	5.00 wt %	10.00 wt %	20.00 wt %
E_{corr}/V	-0.84156	-0.6171	-0.5724	-0.5740	-0.5450	-0.59219
I_{corr}/Acm^{-2}	3.1213×10^{-6}	6.1134×10^{-7}	3.0475×10^{-7}	2.9602×10^{-7}	1.0091×10^{-7}	8.1367×10^{-7}
$R_p/\Omega cm^2$	2.6962×10^5	8.9052×10^5	1.88×10^6	1.89×10^6	1.9357×10^6	1.9203×10^6

The different single-polar coatings (cationic and anionic) exhibit clear superior protective performance than the epoxy varnish coatings (e.g., the much lower corrosion current densities and higher corrosion resistance). This is due to the resisting/blocking ability of the coatings to corrosive ions (Na^+ and Cl^-) resulting from electrostatic repulsion, which is investigated by the ion-selectivity measurements, as shown in Figure 5a. The single-polar, cationic/anionic coatings were placed and fixed between the 3.5 wt % NaCl aqueous solution and the ultrapure water. Measuring the concentration changes of Na^+ and Cl^- of the ultrapure water with increasing time provides information about the ion-selectivity/ion-blocking properties of the single-polar coatings. For cationic coatings (Figure 5b), the concentration of Na^+ is much lower than that of Cl^- throughout the testing time range, which illustrates a good blocking ability of Na^+ . This accounts for the lower corrosion current density of the cationic coatings covering Q235 than that of epoxy varnish. The anionic coatings clearly block Cl^- , as the concentration of Cl^- is much lower than Na^+ during the entire time range (Figure 5c), and this explains the improved anti-corrosion properties of Q235 steel coated with anionic coatings.

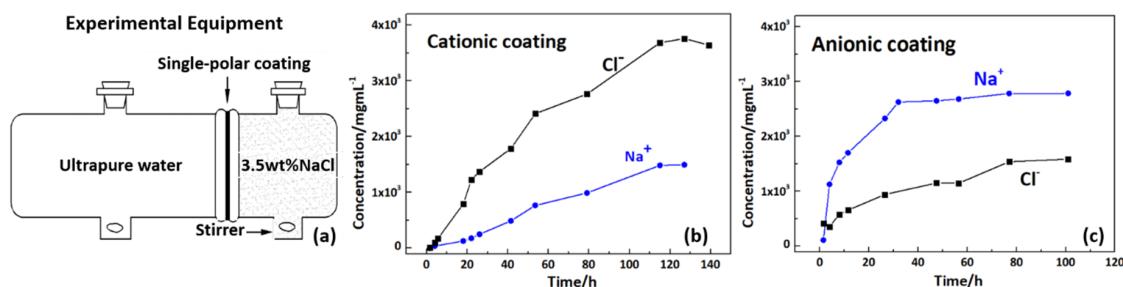


Figure 5. The ion-selectivity of the single-polar coatings. (a) Illustration of the custom-designed experimental equipment. (b) and (c) are the plots of the concentrations of Na⁺ and Cl⁻ in ultrapure water versus increasing time for the cationic and anionic coatings.

Another consideration of the anti-corrosion coatings is the water transmission. The ion-exchange resins could easily absorb water from surroundings, which is not favorable for corrosion inhibition. Our results of the single-polar, cationic, and anionic coatings immersed in 100 mL 3.5 wt % NaCl aqueous solution show significant water uptake (calculated via Equation (1)), which is much higher than the epoxy varnish (Figure 6a). For this, we include an external hydrophobic layer on the single-polar cationic/anionic coating systems in the design. In addition, a high-performance protective coating should control the transport of both the Na⁺ and Cl⁻ ions at the same time. Therefore, we present a design of bipolar, hydrophobic coating system (Figure 6b), which shows our top-down, bio-inspired approach that can block corrosive substances such as water and control transport of corrosive ions within the coating to enhance corrosion protection. The top hydrophobic surface, fabricated by copying the hierarchical structure of microgrooves and micropillars, is shown in Figure 6c, and the contact angle of the water droplet is about 139.1°, which indicates the hydrophobicity.

$$\eta = (w - w_0)/w_0 \tag{1}$$

w- weight of coating at certain immersion times, w₀- weight of the coating before immersion

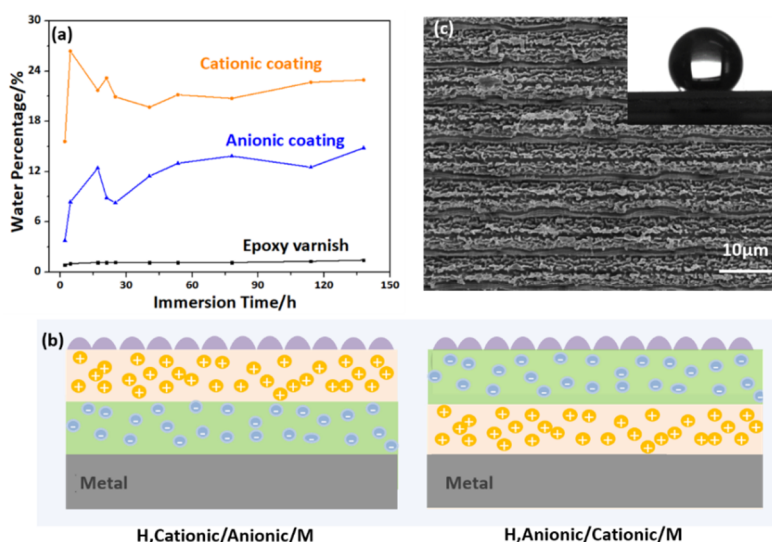


Figure 6. Water absorption property of the coatings, design of bipolar, hydrophobic coatings, and the surface structure of the hydrophobic layer. (a) The water uptake with increasing immersing time of the single-polar and epoxy coatings. (b) The constructed bipolar, hydrophobic coating systems: hydrophobic, cationic/anionic/metal (H, Cationic/Anionic/M) and hydrophobic, anionic/cationic/metal (H, Anionic/Cationic/M). (c) The morphology of the hydrophobic surface with an insert showing the contact angle of a droplet about 139.1°.

3.3. Anti-Corrosion Performance of the Bipolar, Hydrophobic Coating

The representative polarization curves of Q235 with different bipolar, hydrophobic coatings and epoxy varnish after being immersed in 3.5 wt % NaCl solution for 10 days are shown in Figure 7 and the corresponding fitting results are listed in Table 3. For Q235 coated with epoxy varnish, the corrosion current density is 6.1134×10^{-7} A/cm² (Table 3). For Q235 protected by bipolar coatings, the corrosion current density decreased significantly, which indicates a significant increase in anti-corrosion performance. The corrosion current density is only 8.3562×10^{-11} A/cm² for the hydrophobic, anionic/cationic/metal system, and that for the hydrophobic, cationic/anionic/metal system is 1.6966×10^{-11} A/cm², which is more than three orders of magnitude of decrease in the corrosion current density when compared to the epoxy varnish. This demonstrates a substantial enhancement in corrosion protection. The change of polarization resistance is in accordance with the change of the corrosion current density, as shown in Table 3.

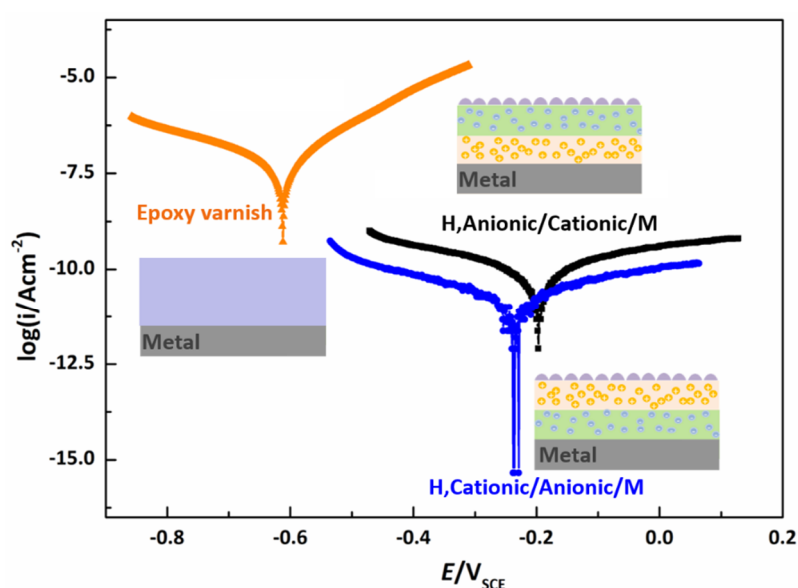


Figure 7. The potentiodynamic polarization curves of different coating systems after being immersed in 3.5 wt. % NaCl aqueous solution for 10 days.

Table 3. Fitting results of Q235 steel coated with the bipolar, hydrophobic coatings and the epoxy varnish after 10 days of immersion.

Parameters	Epoxy Varnish	H, Anionic/Cationic/M	H, Cationic/Anionic/M
E_{corr}/V	-0.6117	-0.1941	-0.2308
I_{corr}/Acm^{-2}	6.1134×10^{-7}	8.3562×10^{-11}	1.6966×10^{-11}
$R_p/\Omega cm^2$	8.9052×10^5	2.3228×10^9	1.3604×10^{10}

Electrochemical impedance spectroscopy was employed to investigate the protective performance of the bipolar, hydrophobic coatings. The impedance modulus $|Z|$ decreased with the increase of immersion time, which indicates that the coating was gradually broken and, thus, the corrosion protection decreased (Figure 8a,b). The corrosion protection of the hydrophobic, cationic coating/anionic coating/metal (H, Cationic/Anionic/M) system was much better than that of the hydrophobic, anionic coating/cationic coating/metal (H, Anionic/Cationic/M) system. This could be attributed to the different degrees in changes of water absorption after applying the hydrophobic surface. The single-polar cationic coatings absorb much more water than the anionic coatings (Figure 6a), and an external hydrophobic surface could lead to a more significant decrease in water uptake, and, thus, a higher increase in corrosion inhibition and anti-corrosion performance enhancement for the H, Cationic/Anionic/M system. Additionally, the impedance modulus $|Z|$ of the H, Cationic/Anionic/M system still remained a high value

after immersion for 10 days (the low frequency range in Figure 8a). For the H, Anionic/Cationic/M system, the impedance modulus $|Z|$ clearly decreased after 1-day immersion, and this decrease was substantial after 10 days, which suggests that the surface was broken. These results indicate that the H, Cationic/Anionic/M system has better anti-corrosion performance than the H, Anionic/Cationic/M system.

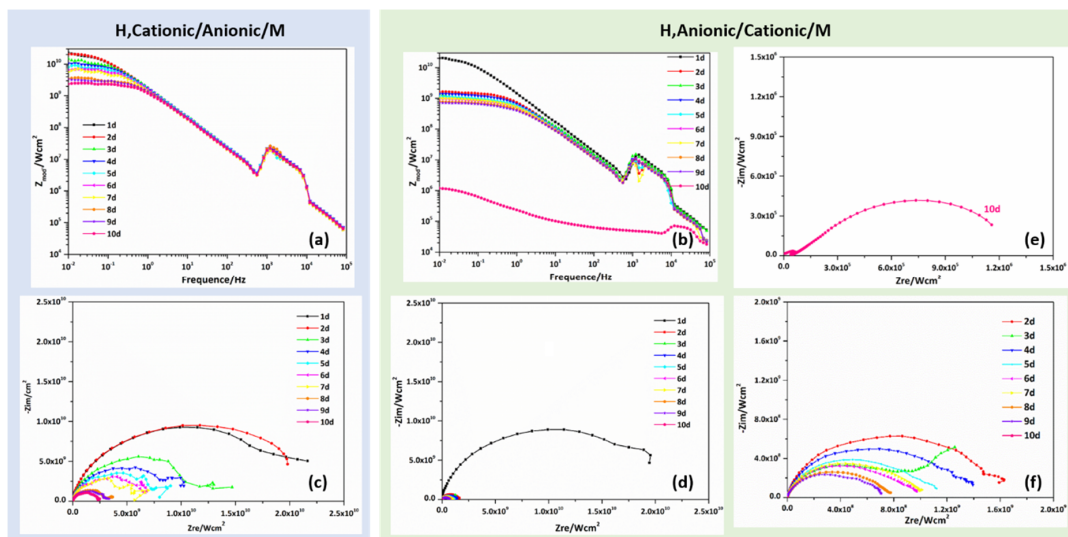


Figure 8. The anti-corrosion capability of the bipolar, hydrophobic coatings during immersion from one to ten days. (a) and (b) are Bode plots of the H, Cationic/Anionic/M system and H, Anionic/Cationic/M system, respectively. (c) is the Nyquist plot of the H, Cationic/Anionic/M system, and (d), (e), and (f) are those of the H, Anionic/Cationic/M system.

The same results can be observed through the Nyquist plots. The results include the impedance change of the different bipolar, hydrophobic coating systems during immersion in 3.5 wt % NaCl solution for 10 days (Figure 8c–f). A large radius of the impedance represents a higher corrosion resistance, and, thus, better anti-corrosion property. Since the radius of the impedance becomes smaller, the anti-corrosion performance of the coatings decreases. Moreover, it is observed that the H, Anionic/Cationic/M system loses protective ability at a faster rate than the H, Cationic/Anionic/M system when comparing the changes of the radius of the impedances. Therefore, the mangrove-inspired, bipolar hydrophobic coatings (H, Cationic/Anionic) can protect the substrate Q235 steel more significantly and for a much longer time.

4. Conclusions

To control the corrosive substances, e.g., water, Na^+ , and Cl^- , is the key for a high-performance anti-corrosion coating to inhibit the corrosion reaction. Strategies developed by nature could provide numerous ingenious designs for dealing with that issue. In this study, we investigated the mangrove salt glands, which are distributed on both surfaces of the leaves (*Ceriops tagal* (perr.) C. B. Rob), and the salt secretion of the salt glands. Inspired by the function of controlling transport of ions into and out of the plant, we designed single-polar and bipolar coatings that have different ion-selective abilities and, thus, control of transport of Na^+ and Cl^- . We further fabricated mangrove-inspired, bipolar hydrophobic coatings that have a top-down protective ability. Our electrochemical evaluations show that, among the manufactured mangrove-inspired protective coatings, the bipolar, hydrophobic coatings (H, Cationic/Anionic) possess significant outstanding and long-term anti-corrosion performance.

Author Contributions: Conceptualization, M.C., Z.W., and B.W. Data curation, M.C., Z.W., and B.W. Investigation and methodology, M.C., Z.W., and B.W. Writing-original draft, M.C. Writing-review and editing, M.C., B.W., Z.W., and P.-Y.W.

Funding: This research received no external funding.

Acknowledgments: B.W. appreciated the financial supports from the Natural Science Foundation of China (No. 51703240) and the Shenzhen Peacock Technology Innovation Fund (No. KQJSCX20180330170430100). Z.W. is grateful for financial support from Shenzhen Science and Technology Innovation Council (JCYJ20170413141208098), Innovation Technology Fund (9440175), Research Grants Council of Hong Kong (No. C1018-17G, No. 11275216), and the City University of Hong Kong (No. 9360140, No. 9667139). P.-Y.W. thanks the supports from the National Key Research and Development Program of China (2018YFC1105201), the general program of National Natural and Science Foundation of China (31870988), the CAS-ITRI cooperation program (CAS-ITRI201902), and the International cooperative research project of the Shenzhen collaborative innovation program (20180921173048123).

Conflicts of Interest: The authors declare no conflict of interest.

References

1. Baeckmann, W.V.; Schwenk, W.; Prinz, W. Handbook of Cathodic Corrosion Protection. *Biochem. Biophys. Res. Commun.* **1997**, *307*, 810–813.
2. Baeckmann, W.V.; Schwenk, W.; Prinz, W. The Invention of Protective Devices. In *Handbook of Cathodic Corrosion Protection*, 3rd ed.; Baeckmann, W.V., Schwenk, W., Eds.; Elsevier: Houston, TX, USA, 1997; pp. 224–229.
3. International Measures of Prevention, Application, and Economics of Corrosion Technologies Study. Available online: <http://impact.nace.org/economic-impact.aspx> (accessed on 1 March 2016).
4. Cui, M.M.; Wang, B.; Wang, Z.K. Nature-Inspired strategy for anti-corrosion. *Adv. Eng. Mater.* **2019**, *21*. [CrossRef]
5. Wang, B.B.; Wang, Z.Y.; Cao, G.W.; Liu, Y.J.; Ke, W. Local corrosion behavior of 2024 aluminum alloy in salt lake atmosphere of western China. *Acta Metall. Sin.* **2014**, *50*, 49–56.
6. Petrov, N.N.; Falina, I.V.; Koval', T.V.; Gorokhov, R.V.; Shel'deshov, N.V.; Bukov, N.N. Electrical-percolation effects in epoxy resin/ion-exchange resin/polyaniline anti-corrosion composite materials. *Prot. Met. Phys. Chem.* **2017**, *53*, 725–732. [CrossRef]
7. Dong, Y.H.; Liu, Y.N.; Zhou, Q. Comparative studies on the corrosion protection effect of different ions selective polyaniline coatings. *Adv. Mater. Res.* **2011**, *287*, 2464–2469. [CrossRef]
8. Dong, Y.H.; Zhang, Q.Y.; Su, X.M.; Zhou, Q. Preparation and investigation of the protective properties of bipolar coatings. *Prog. Org. Coat.* **2013**, *76*, 662–669. [CrossRef]
9. Wang, J.G.; Torardi, C.C.; Duch, M.W. Polyaniline-related ion-barrier anti-corrosion coatings. *Synth. Met.* **2007**, *157*, 846–850. [CrossRef]
10. Couture, G.; Alaaeddine, A.; Boschet, F.; Ameduri, B. Polymeric materials as anion-exchange membranes for alkaline fuel cells. *Prog. Polym. Sci.* **2011**, *36*, 1521–1557. [CrossRef]
11. Lyon, S.B.; Bingham, R.; Mills, D.J. Advances in corrosion protection by organic coatings: What we know and what we would like to know. *Prog. Org. Coat.* **2017**, *102*, 2–7. [CrossRef]
12. Sørensen, P.A.; Dam-Johansen, K.; Weinell, C.E.; Kiil, S. Cathodic delamination of seawater-immersed anticorrosive coatings: Mapping of parameters affecting the rate. *Prog. Org. Coat.* **2010**, *68*, 283–292. [CrossRef]
13. Montoya, R.; García-Galván, F.R.; Jiménez-Morales, A.; Galván, J.C. A cathodic delamination study of coatings with and without mechanical defects. *Corros. Sci.* **2014**, *84*, 432–436. [CrossRef]
14. Kalendová, A. Effects of particle sizes and shapes of zinc metal on the properties of anticorrosive coatings. *Prog. Org. Coat.* **2003**, *46*, 324–332.
15. Wang, Z.C.; Zhang, Y.Z.; Gu, Z.J. A study on anti-corrosion performance of ion-selective phenolic coatings for carbon steel by EIS. *Mater. Prot.* **1998**, *31*, 1–4.
16. Wang, Z.C.; Gu, Z.J. Corrosion behaviour of copper covered with ion-selective phenolic coatings by EIS. *ElectroChemistry* **1997**, *3*, 271–276.
17. Wang, Z.C.; Gu, Z.J. Electrochemical and corrosion behaviour of A3 steel covered with ion-selective organic coating. *J. Xiamen Univ.* **1997**, *36*, 387–393. (In Chinese)
18. Pereira da Silva, J.E.; Córdoba de Torresi, S.I.; Torresi, R.M. Polyaniline acrylic coatings for corrosion inhibition: The role played by counter-ions. *Corros. Sci.* **2005**, *47*, 811–822. [CrossRef]
19. Wang, H.L.; Liao, S.Y. Salt glands and epidermal non-glandular hair structures in mangrove and coastal plants in DaYa bay. *J. Oceanogr. Taiwan Strait* **2000**, *19*, 372–378.

20. Fu, X.M.; Su, L.R.; Wang, X.Y. A study on the framework of blance sheet of marine biological resources. *Pac. J.* **2017**, *25*, 104.
21. Hao, C.L.; Li, J.; Liu, Y.; Zhou, X.F.; Liu, Y.H.; Liu, R.; Che, L.F.; Zhou, W.Z.; Sun, D.; Li, L.; et al. Superhydrophobic-Like tunable droplet bouncing on slippery liquid interfaces. *Nat. Commun.* **2015**, *6*, 7986. [[CrossRef](#)]
22. Liu, C.R.; Sun, J.; Xiang, C.H.; Che, L.F.; Wang, Z.K.; Zhou, X.F. Long-Range spontaneous droplet self-propulsion on wettability gradient surfaces. *Sci. Rep.* **2017**, *7*, 7552. [[CrossRef](#)]
23. Liang, W.L.; Ma, X.L.; Wan, P.; Liu, L.Y. Plant salt-tolerance mechanism: A review. *Biochem. Biophys. Res. Commun.* **2018**, *495*, 286–291. [[CrossRef](#)] [[PubMed](#)]
24. Tan, W.K.; Lin, Q.S.; Lim, T.M.; Kumar, P.; Loh, C.S. Dynamic secretion changes in the salt glands of the mangrove tree species *avicennia officinalis* in response to a changing saline environment. *Plant Cell Environ.* **2013**, *36*, 1410–1422. [[CrossRef](#)] [[PubMed](#)]
25. Tyerman, S.D. The devil in the detail of secretions. *Plant Cell Environ.* **2013**, *36*, 1407–1409. [[CrossRef](#)] [[PubMed](#)]
26. Deinlein, U.; Stephan, A.B.; Horie, T.; Luo, W.; Xu, G.; Schroeder, J.I. Plant salt-tolerance mechanisms. *Trends Plant Sci.* **2014**, *19*, 371–379. [[CrossRef](#)]
27. Dassanayake, M.; Larkin, J.C. Making plants break a sweat: The structure, function, and evolution of plant salt glands. *Front. Plant Sci.* **2017**, *8*, 406. [[CrossRef](#)]



© 2019 by the authors. Licensee MDPI, Basel, Switzerland. This article is an open access article distributed under the terms and conditions of the Creative Commons Attribution (CC BY) license (<http://creativecommons.org/licenses/by/4.0/>).